

Measurements of Organized Turbulence in the Dual-Phase Flow Below a Rotor

Jürgen Rauleder*

J. Gordon Leishman†

Department of Aerospace Engineering
University of Maryland, College Park, MD 20742

Time-resolved particle image velocimetry and particle tracking velocimetry measurements of the flow field were made below a laboratory-scale rotor hovering in ground effect over a mobile sediment bed. Single-phase and dual-phase measurements were compared to examine how the mean flow, turbulence fields, and coherent vortex structures were modified by the uplifted particles contained within the dispersed-phase. The helicoidal blade tip vortices were tracked in the flow as they developed, diffused and reintensified while convecting over the ground plane. It was found that the vortex flows were distorted by the particles, accelerating the processes of diffusion and vortex break-up. The two-phase flow contained a more complicated vorticity field with smaller length-scales in the environment near the ground. The mean flow and turbulence characteristics were modified by the particles close to the sediment bed but also further away from the ground where they produced turbulence and increased the anisotropy of the turbulence. The results also give a better understanding of the boundary conditions that would be required for the development and validation of models used for the simulation of the complex turbulent two-phase flows typical of rotorcraft brownout conditions.

1. NOMENCLATURE

c	Rotor blade chord
C_T	Rotor thrust coefficient, $= T/\rho\pi\Omega^2R^4$
k	Turbulent kinetic energy (in 2-d), $= \frac{1}{2}(\overline{u'^2} + \overline{v'^2})$
N_b	Number of rotor blades
r	Radial distance measured from rotor axis
R	Rotor radius
Re_c	Chord Reynolds number, $= V_{tip}c/\nu$
Re_{max}	Wall jet Reynolds number, $= u_{max}z_{max}/\nu$
Re_v	Vortex Reynolds number, $= \Gamma_v/\nu$
t	Time elapsed after rotor blade passage
T	Rotor thrust
T_u	Streamwise turbulence intensity, $= \sqrt{\overline{u'^2}}/v_h$
T_v	Wall-normal turbulence intensity, $= \sqrt{\overline{v'^2}}/v_h$
u, v	Flow velocities in r and z directions, respectively
\bar{u}, \bar{v}	Mean velocities in r and z directions, respectively
u', v'	Fluctuation velocities in r and z directions
u_{max}	Maximum flow velocity of wall jet
v_h	Hover induced velocity, $= \sqrt{C_T}/2$
V_{tip}	Rotor tip speed, $= \Omega R$
z	Distance from the ground

z_{max}	Distance of maximum velocity from wall
Γ_v	Vortex circulation
ζ	Wake age, $= \psi_b + \Omega t (180^\circ/\pi)$
μ	Dynamic viscosity
ν	Kinematic viscosity, $= \mu/\rho$
ρ	Air density
σ	Rotor solidity, $= N_b c/\pi R$
ψ_b	Blade azimuth angle
Ω	Rotational speed of the rotor

2. INTRODUCTION

Brownout conditions occur when a dense dust cloud develops around a rotorcraft as it takes off, lands, or hovers over surfaces covered with loose sediment, such as found in arid or desert operating environments. The high concentrations of suspended dust particles in such conditions can cause severe visual obscurations and motion cue anomalies that affect the pilot's ability to safely fly the helicopter. The occurrence of brownout has been reported to be a leading cause of human factor-related helicopter mishaps in military [1] operations, and civilian operators too have suffered consequences [2]. Improved sensors and avionics to "see" through the dust clouds, combined with operational tactics, have helped somewhat to reduce the frequency of brownout-related mishaps. However, in the longer term an improved understanding of the fluid dynamic factors that influence brownout and the exploration of strategies to mit-

*Ph.D. Student. juergenr@umd.edu†Minta Martin Professor. leishman@umd.edu

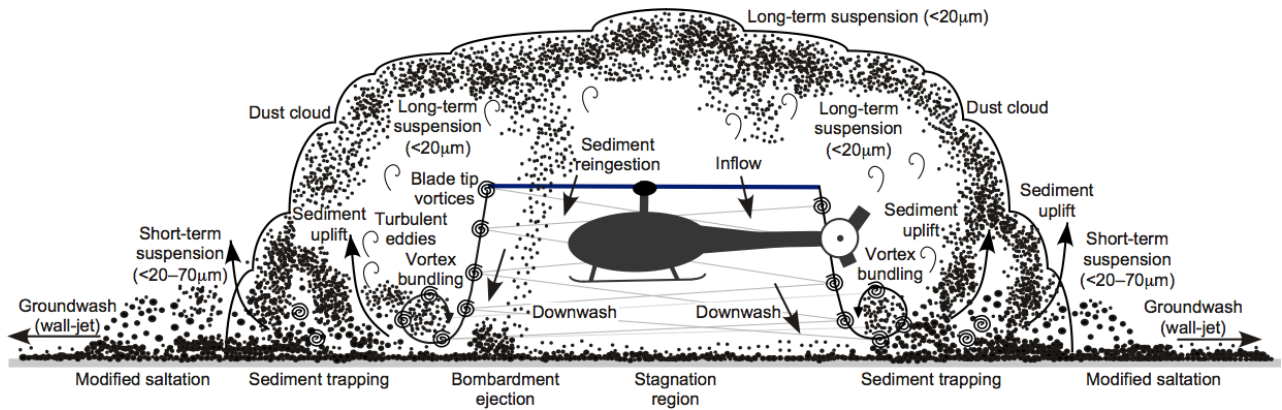


Fig. 1: Schematic showing different modes of particle uplift and particle motions generated by a helicopter encountering brownout conditions.

igate its severity will be needed to ensure safe and cost-effective rotorcraft operations.

Underlying the physics of the brownout problem are highly three-dimensional unsteady, turbulent, dual-phase fluid dynamics. The dual-phase nature of the problem arises because the fluid (or carrier) phase flow field produced by the intense rotor wake causes sediment particles from the ground to be picked up and entrained into the flow around the rotor. Some of the mechanisms that lead to sediment uplift and transport in the flow field near a helicopter operating in ground effect conditions are illustrated in Fig. 1. It has been suggested that if the generation of brownout and the underlying fluid dynamics that lead to particle mobilization and uplift can be better understood, then a predictive capability could be developed [3, 4], perhaps making brownout mitigation possible through the process of rotorcraft design [5–7].

Recent experimental studies have begun to better expose the fluid dynamic details of the single-phase flow near the ground below hovering rotors; see [5, 8]. Such flow fields contain the coherent tip vortices and vortex sheets created at the rotor blades, as well as eddies and small-scale turbulence, thereby producing a highly complex flow environment at the ground with intermittent characteristics; see Fig. 2. Measurements have also been made of the dual-phase heterogeneous flow environment near a sediment bed below a rotor [9–11]. High surface shear stresses, combined with velocity fluctuations and the turbulent Reynolds stresses, discrete turbulence events, local pressure gradients, and the unsteady upward flow velocities induced by the tip vortices, lead to the pickup and suspension of sediment particles [12]. Any suspended particles can then be convected by the turbulent, unsteady, vortical flow surrounding the rotor. The smaller and lighter particles trapped in the stronger vortical flow regions may also be recirculated back onto the sediment bed, ejecting more particles by bombardment mechanisms, and so rapidly intensifying the total quantity of suspended particles [11, 13].

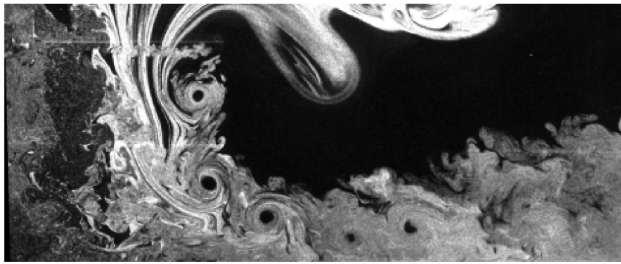
Despite the abundance of particle-laden flows in both nature and industry, a generally applicable theory or model

for predicting the behavior of such two-phase flows is currently unavailable. This situation arises because of the lack of consistent experimental data that is available for both model formulation and validation purposes [14]. Even for more canonical dual-phase flows, measurements and predictions of straightforward metrics such as the turbulent kinetic energy show contradictory results; see [15] for an overview. For more complex, vortically-dominated flows, such as found in the flow near a helicopter rotor, detailed quantitative assessments of the combined two-phase flow characteristics by the addition of a dispersed particle phase do not yet exist.

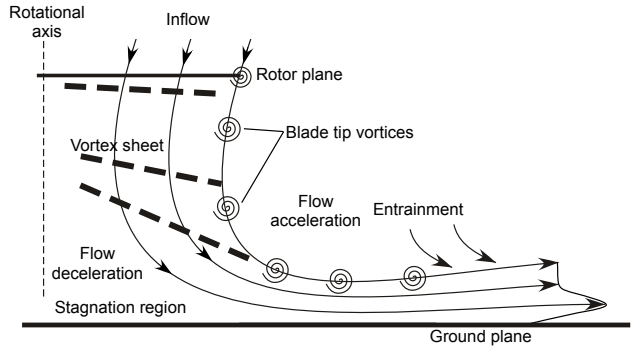
If high enough particle concentrations in the flow build up, thereby changing the particle volume and mass load (and possibly other flow properties as well), then the flow structure and the turbulence properties of the carrier (or continuous) phase may be modified [16, 17]. This means that the problem becomes two-way coupled (i.e., the particles affect the carrier-phase flow), or even four-way coupled (particle/particle interactions become important). A coupling between the phases further increases the complexity of the dual-phase flow problem, especially from a modeling perspective.

It is because of the lack of experimental data that the validation of predictive dual-phase models has been held back. Such models should also include interphase turbulence transfer terms for turbulence modulation [18]. In the absence of sufficient experimental data, turbulence models used in CFD simulations of two-phase flows merely employ simple extensions of the standard single-phase $k - \epsilon$ model, which may not be correct; see e.g., Montante and Magelli [19].

Results from channel flow experiments [20, 21] and other types of more canonical solid/liquid and solid/gaseous dual-phase flows have already exposed that the particle phase can affect the flow properties of the fluid phase to a lesser or greater degree. Zhang et al. [22] investigated the effects suspended sand particles have on the wind field found in the desert. Depending on the particle size, as well as the mass and volume fraction of the particles in



(a) Flow visualization image



(b) Schematic of the flow

Fig. 2: Flow features in the rotor wake developing in ground effect shown by: (a) flow visualization, (b) corresponding schematic of the flow characteristics.

the flow, the dispersed-phase may produce or suppress the turbulence of the carrier-phase. Poelma et al. [14] showed that suspended particles can produce turbulence and that the dispersed-phase can increase the anisotropy of the turbulence. However, these results are not necessarily universal because they will depend not only on the particle volume fraction, but also on the type of flow. Therefore, results found, for example, in a channel flow with particles suspended in water, may not be applicable to the complex flow environment produced by a rotor where many particles are picked up from the ground by vortical flow features.

It has been recognized that turbulence plays an important role in particle mobilization by the wind [23–25], and that turbulence events (or organized turbulence) are primarily responsible for the initiation of sediment motion [26, 27]. However, turbulence effects on particle mobilization have not yet been modeled satisfactorily [28]. In this regard, sediment transport and particle uplift models, such as the well-known models of Bagnold [23] and Shao and Lu [29], do not explicitly account for the effects of turbulence and unsteadiness in the flow. These models also do not account for the possibility that particles can alter the carrier-phase, affect the coherent flow structures, and modify the turbulence. Such modifications to the fluid flow properties may then, in turn, influence particle pickup and entrainment. From experiments, Xuan [28], Williams [30], and Xuan and Robins [31], concluded that turbulence may significantly influence dust mobilization and the resulting particle mass flux.

It has yet to be shown whether the effects of two-way coupling are important for simulating rotor flows near the sediment-covered ground and/or further away from the sediment bed (i.e., permitting the application of simplified one-way coupling models). Rauleder and Leishman [12] showed how the Reynolds stresses, concentrated vorticity (such as the tip vortices), and turbulence events of the fluid phase affected sediment mobilization, pickup, and subsequent entrainment of particles from a sediment bed below a rotor. These results from time-resolved, dual-phase flow measurements have better exposed the complex interplay

between the carrier and dispersed phases in a rotor flow environment. The Reynolds stress distribution of the carrier near the ground was found to be altered by the presence of suspended sediment particles in the flow, even at relatively sparse particle concentrations. While these were the first experimental time-resolved studies of turbulence modification by solid particles in the flow below a rotor, only a region very close to the ground was analyzed; see [12].

It is clear that more comprehensive comparative single-phase/dual-phase results are necessary for the validation of the numerical models. Therefore, new experimental results must be obtained to quantify to what degree the addition of a dispersed-phase in the flow modifies the turbulence characteristics of the carrier-phase in the near-wall flow on the ground below a rotor. To this end, the objectives of the present work were to measure how the addition of a dispersed solid particle phase alters the turbulence characteristics of the carrier-phase, and to quantify how the particles may change the organized turbulence and the coherent vortex structures. Another objective was to provide useful approximations and boundary conditions for the development and validation of models used for the simulation of two-phase vortical flows and, thus, for the modeling of rotorcraft brownout conditions.

3. DESCRIPTION OF THE EXPERIMENT

3.1 Time-Resolved Dual-Phase Flow Measurements

The experiments were conducted using a two-bladed rotor system with a radius of 0.085 m (0.279 ft). Thin, cambered airfoils with a sharpened leading edge and a chord of 0.018 m (0.059 ft) were used for the rotor blades. The rotor was placed with its rotational plane at a height of one rotor radius above a ground plane; see Fig. 3. The rotor was operated at a nominal rotational frequency of 60 Hz (3,600 rpm), which corresponded to a blade tip speed of 32.04 ms^{-1} (105.12 ft s^{-1}) and a tip chord Reynolds number, Re_c , of approximately 35,000. The blade pitch was set to produce a representative blade loading coefficient,

C_T/σ , of 0.0136 in ground effect. This blade loading produced a tip vortex with a measured circulation (i.e., vortex strength) of $\Gamma_v = 0.0172 \text{ m}^2\text{s}^{-1}$ ($0.185 \text{ ft}^2\text{s}^{-1}$) giving a vortex Reynolds number of $Re_v = 1,100$. The hover induced velocity from rotor theory [32] was calculated to be $v_h = \sqrt{C_T/2} = 3.3 \text{ ms}^{-1}$ (10.8 ft s^{-1}).

Single-phase and dual-phase time-resolved flow field measurements below the rotor were analyzed to study the two-way coupling between the phases, i.e., how the addition of a dispersed particle phase may alter the flow field generated by the rotor near the ground. In particular, it was investigated to what degree the particles modify the turbulence quantities and coherent flow structures in the vortically-dominated flow near the sediment bed, as well as further away from the ground. All of the flow measurements were performed using particle image velocimetry (PIV) for the single-phase flows and for the carrier-phase in the dual-phase experiments, while particle tracking velocimetry (PTV) was used to measure the velocities of the sediment particles in the dispersed-phase.

A high-speed 1 MP CMOS camera and Nd:YLF dual-laser system were used to perform the PIV and PTV. The laser and the camera were digitally synchronized and controlled by a timing hub. The laser beam was passed through cylindrical and spherical lenses to create a thin, diverging light sheet that had a thickness of approximately 1 mm in the interrogation region. The system was capable of capturing image pairs at 1,500 Hz at full camera resolution, and allowed for a contiguous time-history of the flow to be recorded. However, a frame rate of 1,000 fps was found to be satisfactory for balancing the temporal resolution needed to track the coherent vortex structures and the displacements of the sediment particles, with the image intensity needed to perform successful cross-correlations with the image pairs.

The laser pulse separation time was set to $15 \mu\text{s}$, which proved to be a good balance for accurately measuring the flow velocities and particle displacements while the out-of-plane losses were minimized by the relatively small pixel displacements. In each run, 500 sequential image pairs were obtained, which corresponded to 30 rotor revolutions. A hyper-streaming system was used to buffer the large quantity of data before transferring it to a computer for subsequent image processing and analysis.

For the dual-phase experiments, the particles were loosely deposited over the ground plane forming a mobile sediment bed of a thickness of 11 mm (0.433 in). Well-characterized glass microspheres with a diameter of 45–63 μm were used, and the surface of the bed made smooth with a scraper. Experiments with smaller and bigger particles were also performed, however, the 45–63 μm glass microspheres were found to give the best trade between the necessary particle mobility and a particle oversaturation of the recorded images. On one hand, oversaturation occurs when the particles are uplifted too easily from the sediment bed, giving concentrated bursts of particles and

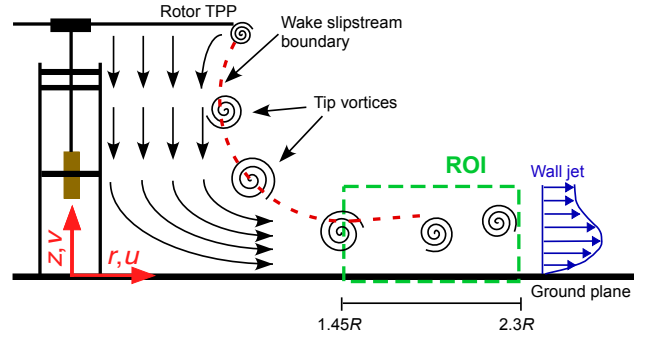


Fig. 3: Schematic showing the smaller rotor system used for both the single-phase and dual-phase flow measurements.

making it difficult to detect and track individual particles with the PTV algorithm. On the other hand, if the particles are too large, then the quantity of individual particles being uplifted over time is insufficient to give a statistically meaningful particle quantification, as it would be needed for measuring the local particle flux.

3.2 Image Processing and Analysis

The analysis of the single-phase and carrier-phase measurements were performed using standard PIV cross-correlation algorithms. The images were first spatially calibrated. Masking was used for the regions adjacent to the ground. A multipass method with square interrogation windows was used and a deformation grid implemented. The initial interrogation window size was 40-by-40 pixels, with a final window of 24-by-24 pixels. To further refine the PIV cross-correlations, two passes of the Rohaly-Hart analysis were used. Each vector was validated using universal median and signal-to-noise tests. All processed images used for subsequent analysis contained less than 5% spurious vectors. This approach permitted measurements with good spatio-temporal resolution to resolve the coherent vortex structures in the flow, and also allowed the small-scale fluctuations from turbulence to be resolved.

The dual-phase flow measurements required clean phase separation before the individual velocities of the carrier and dispersed phases could be resolved. As the sizes of the sediment particles and the tracer particles (mineral oil-based with average diameter of $0.2 \mu\text{m}$) were more than two orders of magnitude different, the dispersed-phase could be distinguished from the carrier-phase tracer particles by using a size and brightness thresholding method. An optimum intensity gray scale threshold for the images was determined, and pixels above this threshold were subtracted from the raw images thereby yielding separate carrier-phase and dispersed-phase images [11]. The carrier-phase with the submicron seed particles was then analyzed using conventional PIV techniques, as previously described.

In the dual-phase measurements, the carrier-phase images contained some masked holes, which is a consequence

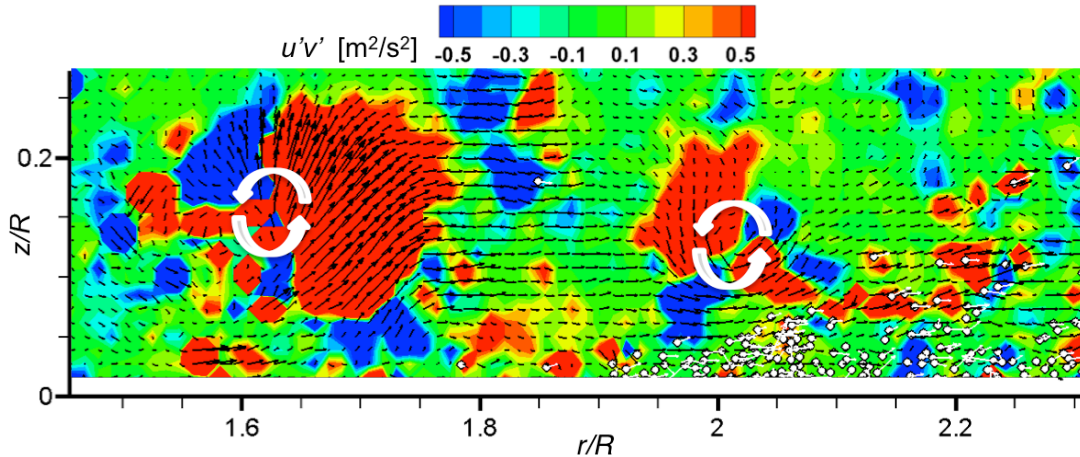


Fig. 4: Dual-phase flow realization above the sediment bed showing instantaneous velocity vectors of carrier and dispersed phases on a background contour of instantaneous Reynolds shear stress, also depicting the positions of the tip vortices.

of the subtraction of the dispersed-phase. In addition, the flow under investigation was vortically dominated, and so any residual analysis for vector validation based on the global mean velocities is impractical because it would not take the local coherent motion into account. For these reasons, a 3-by-3 local median test was performed to assess the validity of the velocity vectors, replace them, and re-supply any masked holes with the local median (instead of the local or global mean).

The dispersed-phase analysis (which contains relatively sparse numbers of particles compared to the carrier-phase) was then performed using PTV. The PTV algorithm identified individual sediment particles by the size and brightness thresholding method explained previously, and tracked them across each PTV image pair. From the particle displacements, the velocities for each particle could then be calculated based on the known laser pulse separation time. Finally, the carrier-phase PIV and dispersed-phase PTV measurements were recombined to produce the net dual-phase flow field. This form of analysis yielded accurate quantitative simultaneous measurements of both phases of the flow.

4. RESULTS AND DISCUSSION

Comparative single-phase and dual-phase rotor experiments were analyzed to examine how the mean flow properties, turbulence fields, and coherent vortex structures (such as the rotor blade tip vortices), were affected by the dispersed-phase particles uplifted from the sediment bed; see Fig. 4. A contiguous time-history of the flow as it developed over the ground plane was obtained. The resolution of the PIV system used in the present work was such that the dual-phase environment could be resolved with good spatio-temporal detail. Coherent vortex structures were tracked as they developed, diffused, and intensified while convecting toward the ground plane. Such a

comparison made it possible to assess how the mean flow, vorticity, and turbulence of the carrier-phase were modified by the presence of the sediment particles.

Figure 4 shows an instantaneous planar realization of the dual-phase flow environment generated by the rotor. Also shown are the locations of the coherent tip vortices, which are of expanding helicoidal form near the ground. The signature of the tip vortex seen further downstream at $r/R = 2.0$ shows a distinct quadrupole (or four-lobed) structure that is associated with coherent vortices when shearing stresses (or strain rates) are analyzed in a Cartesian coordinate system [33, 34]. Beside the concentrated vorticity, smaller-scale $u'v'$ correlations that indicate small vortex structures, eddies, and secondary flow structures, were also present. The latter were induced through the interaction of the primary vortex structures with the ground, or by interactions between the vortices themselves. The occurrence of such small-scale vortical structures was found to be more frequent in the dual-phase flow environment; see also a comparison of Figs. 7 and 8.

In the region of interest (ROI) depicted in Fig. 3, the sediment particles were detected and counted by the PTV algorithm. Therefore, particle concentration and flux measurements could be performed to quantify sediment transport. The particle volume fraction in the ROI was measured to be 10^{-4} . According to Poelma et al. [14], this volume fraction is in the so-called “two-way coupled” regime where there is likely to be interactions between the particles and the fluid, yet the load is low enough to neglect particle/particle interactions.

Elghobashi [35] classified three coupling regimes between the phases on the basis of the particle volume fraction in the fluid. For a volume fraction less than 10^{-6} , the presence of the particles has a negligible effect on turbulence and the interaction between the particles and turbulence is “one-way coupled.” For a volume fraction between 10^{-6} and 10^{-3} , the momentum transfer from the

particles is large enough to alter the turbulence structure and turbulence modifications may occur, also depending on other flow parameters. This interaction is termed “two-way coupled.” For a volume fraction greater than 10^{-3} , particle/particle collisions become important and the turbulence of the carrier-phase can also be affected by such collisions, which is termed “four-way coupled.”

4.1 Mean Velocities in the Single- and Dual-Phase Flow

Notice from Fig. 3 that the flow from the rotor disk turns from a mostly vertical (toward the wall) direction to a mostly wall-parallel flow as it develops to a jet-like flow along the ground plane, but still contains the discrete vorticity induced by the tip vortices; see Fig. 5. The Reynolds number based on the maximum velocity at the ground and the wall-normal distance where this maximum occurred was measured to be $Re_{\max} = u_{\max} z_{\max} / \nu = 7,000$.

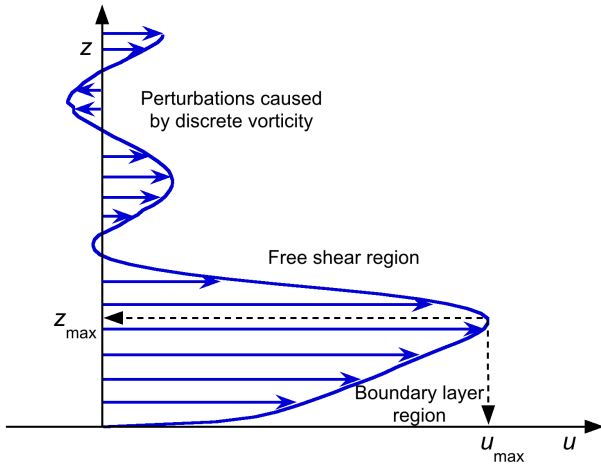


Fig. 5: Representative near-wall mean flow as found below a rotor.

The mean wall-parallel flow velocity profiles are shown in Fig. 6 for two locations downstream from the rotor for both the single-phase and the carrier in the dual-phase flow. These two experiments were conducted under the same rotor operating conditions (same rotor thrust, blade loading, etc.). Time-averaging was performed over all blade azimuth positions after a contiguous time-history containing 500 consecutive vector fields was obtained.

The mean velocity profiles obtained for the near-wall flow below the rotor clearly appeared to be similar to those of a developing turbulent wall jet [36]. Canonical flows such as channel or pipe flows certainly contain organized turbulence structures in the near-wall region [37]. However, the initial source of turbulence in such flows is not the more concentrated vorticity as seen here with the rotor flow. Therefore, at least some differences in the near-wall turbulence structures are to be expected for these reasons alone. Downstream, measurements of the dual-phase flow (solid lines) could not be made as close to the ground

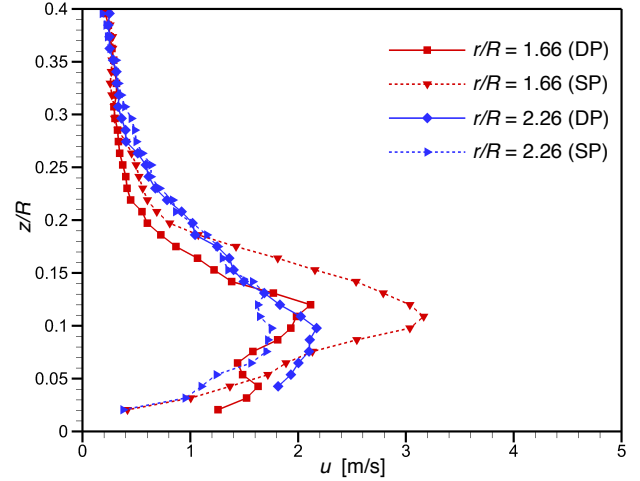


Fig. 6: Mean wall-parallel velocity profiles for the fluid phases at two downstream distances from the rotor.

as for the single-phase flow (dashed lines) because of laser light reflections from the bed.

At the ground, the velocities were found to be greater when the dispersed-phase was included in the flow. The particles caused more vigorous turbulent mixing and enhanced energy transfer near the wall, causing an increase in the rate of strain and the velocity gradient adjacent to the wall, thereby also increasing the friction velocity. This result is consistent with findings for more canonical flows, e.g., for a channel flow with water and a solid particle phase such as conducted by Kiger et al. [21].

While a large difference in the single- and dual-phase velocity profiles could be observed for the measurement location upstream ($r/R = 1.66$; red lines), the differences were found to be much less pronounced further downstream ($r/R = 2.26$; blue lines); see Fig. 6. This finding suggested that the augmented turbulent mixing and energy transfer caused by the particles produced a faster redistribution of kinetic energy in the flow as it developed along the ground. At locations further downstream, however, the near-wall flow was fully developed such that the velocity profiles for the single- and dual-phase flows were more similar.

4.2 Vortical Structure of the Flow

Figures 7 and 8 show instantaneous flow realizations of the single- and the dual-phase flows, respectively. Instantaneous velocity vectors are shown on background contours of vorticity magnitude for every sixth flow realization, i.e., every sixth time step of the contiguous time-history. With a recording frequency of 1,000 Hz, the results are separated by 6 ms or 130° in terms of wake age. The wake age, ζ , of a vortex is the time (in degrees) that has passed between the current realization and the point in time it was produced at the blade. The image sequences were chosen such that at the starting point of the time series, the primary tip vortices

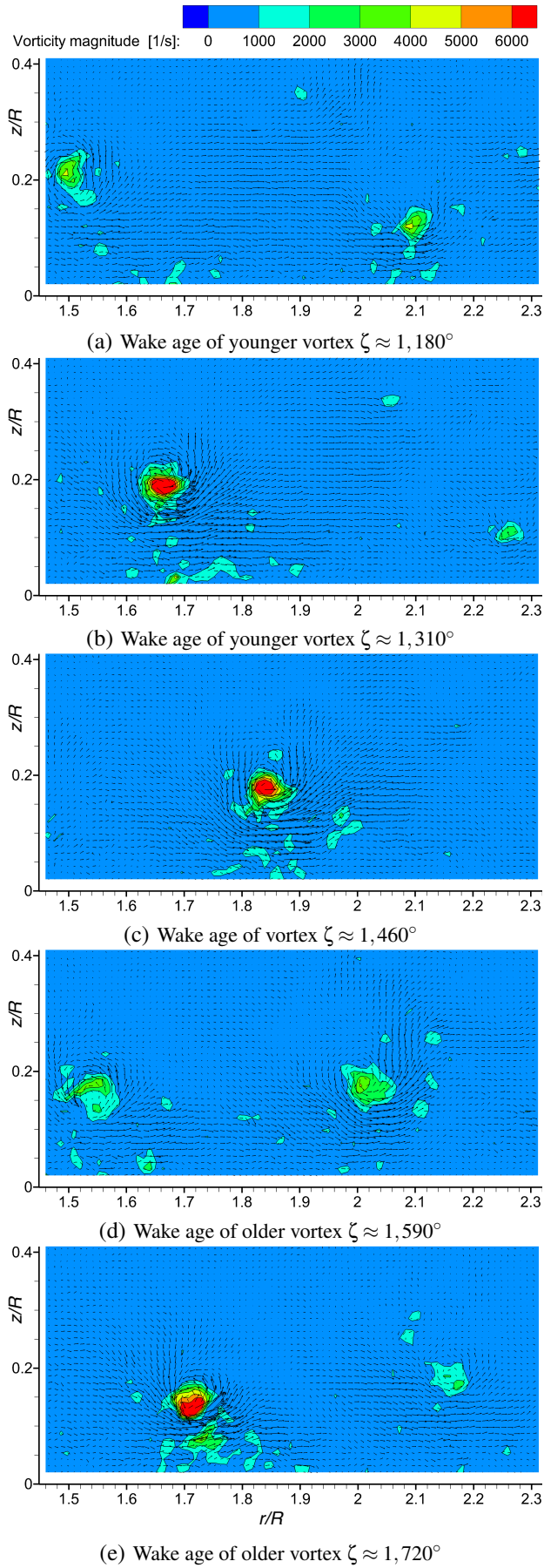


Fig. 7: Sequence of instantaneous single-phase flow realizations showing every sixth measured vector field.

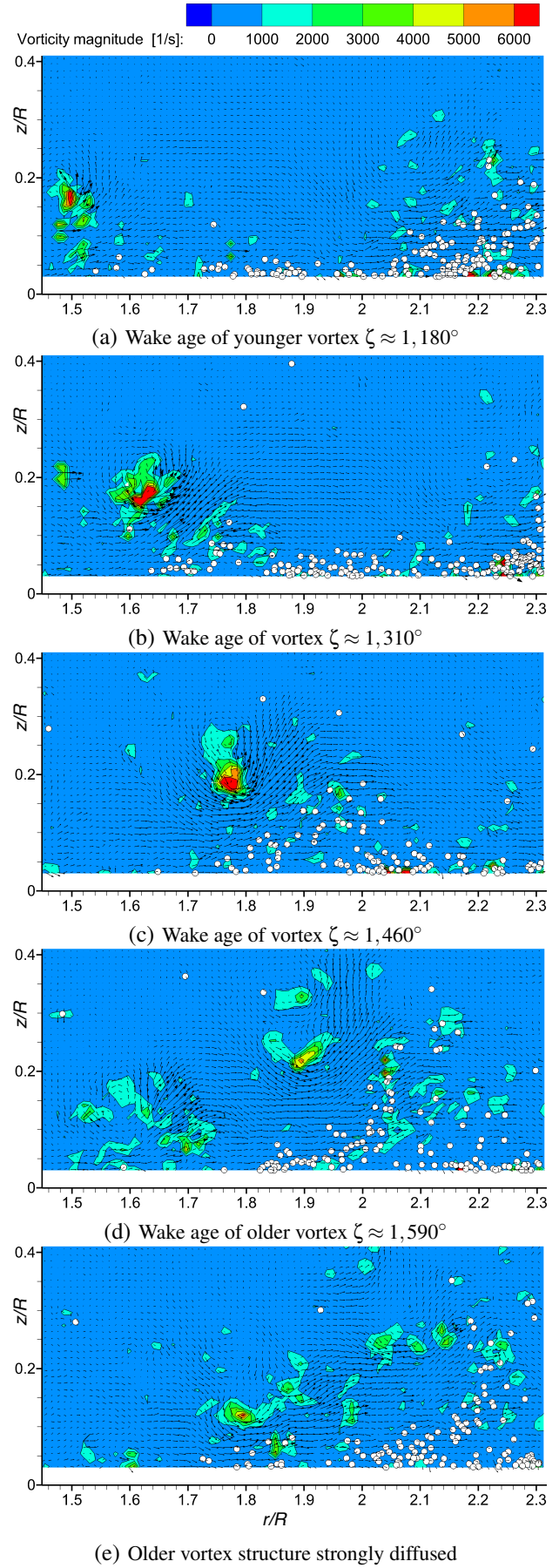


Fig. 8: Sequence of instantaneous dual-phase flow realizations showing every sixth measured vector field.

were approximately at the same downstream distance from the rotor for both the single- and the dual-phase flows.

From the first three flow realizations (a)–(c), it can be seen that with and without a dispersed-phase, an intensification of the vorticity contained in the tip vortices occurred as they convected downstream [33]. Furthermore, in the field of view shown here the tip vortices convected under the influence of the near-wall flow, which is becoming a wall jet-like flow. As the tip vortices convected along the slipstream boundary (or shear layer) between the accelerated flow near the wall and the more quiescent flow further away from the wall, they experienced a stabilizing (if not intensifying) effect through the action of the wall jet because their rotational flow is augmented by the accelerated mean flow at the ground.

The carrier in the dual-phase flow showed more compact contours of relatively larger vorticity, but these pockets of greater-than-average vorticity were distributed over a wider part of the ROI. While the vorticity was more concentrated in the discrete tip vortices in the single-phase flow, the concentrated vorticity in the dual-phase flow was noted to diffuse more quickly into smaller vortical structures. From (e)–(f), it can be seen that the vortices in the single-phase flow were coherent even beyond $r/R = 2$, while the vortices in the dual-phase flow have mostly lost their coherent structure. Furthermore, notice that the overall structure of the carrier-phase became more complicated in regions where larger quantities of particles were suspended in the flow.

Comparing Figs. 7 and 8 shows that the distortion or diffusion of the large-scale vortex structures in the dual-phase flow takes place primarily in regions of high particle concentrations, and so it can be attributed to the presence of the uplifted particles. This distortion, and the quicker break-up of coherent flow structures by the particles, yielded a vorticity field with smaller length scales in the particle-laden case (Fig. 8), which also causes a more rapid energy transfer to the small-scale vortical structures. This result is consistent with the findings of Eaton [38], who investigated turbulence modification by particles in shear flows, and also with Poelma et al. [14] who studied a dual-phase flow in a pipe with grid-generated turbulence.

4.3 Turbulence Intensities and Production

Although Reynolds-averaging techniques do not explicitly account for coherent motions in the turbulence, some instantaneous organization is apparent even in the averaged terms. The turbulence intensity is a measure of the effect turbulent structures such as eddies and larger coherent vortical structures have on the mean flow. Sediment motion arises, at least in part, from the velocity fluctuations, turbulence intensities and turbulent (Reynolds) stresses [23].

The fluctuating parts of the flow velocities were extracted from the measurements, which were then used for

the computation of the turbulence quantities. By performing a classic Reynolds decomposition, then the fluctuation (or perturbation) velocities are

$$u'_{i,j} = u_{i,j} - \overline{u_{i,j}} \quad (1)$$

$$v'_{i,j} = v_{i,j} - \overline{v_{i,j}}, \quad (2)$$

respectively. In this case, $u'_{i,j}$ is the fluctuation velocity at a single interrogation point, $u_{i,j}$ is the instantaneous velocity at this point, and $\overline{u_{i,j}}$ is the average u velocity. The average velocity components were calculated using

$$\overline{u_{i,j}} = \frac{1}{N} \sum_{k=1}^N u_{i,j}(k), \quad (3)$$

where N is the number of contiguous PIV realizations. A similar equation holds for the v component.

As a measure of the strength of turbulence, the turbulence intensities in the streamwise and wall-normal directions, T_u and T_v , and the turbulent kinetic energy, k , were calculated from the measured velocity fluctuations; see Figs. 9, 10, and 11, respectively. In the dual-phase results, the extremely high values for these turbulence quantities downstream of $r/R \approx 2.1$ just above the sediment bed are erroneous because of the loss of carrier-phase information when particle concentrations become too high, causing significant laser light reflections.

As discussed previously, the flow at the ground below the rotor was dominated by concentrated vorticity contained in the blade tip vortices. The vortices induced significant local velocity fluctuations, and the increased turbulence levels in the near-wall region were also mainly because of these vortices. As also discussed, the concentrated vorticity contained in the vortices was reintensified by stretching effects between $r/R = 1.45$ – 1.80 as the vortices convected downstream over the ground. Such intensification was found to be more pronounced for the single-phase flow. It is also this reintensification of the vortices that caused the elongated distribution of T_u , T_v , and k , as seen in Figs. 9, 10, and 11, respectively.

It is apparent that the distributions of turbulence intensity in the dual-phase flow are different from those measured for the single-phase flow, the former showing greater values closer to the sediment bed. Further away from the bed, the turbulence intensities were also greater in the dual-phase flow, but only in regions downstream where most sediment particles were suspended; also compare to Figs. 8, 13, and 14. For both the single- and dual-phase flows, the streamwise component T_u was greater than T_v very close to the ground plane (or the sediment bed in the dual-phase flow), while it was smaller than T_v further away from the ground.

The term describing turbulence production in the energy equation for turbulent flows can be written as $-\overline{u'v'} \left(\frac{\partial \overline{u}}{\partial z} \right)$. Its values are shown in Fig. 12. Turbulence production by the action of the tip vortices extended to greater radial distances from the rotor for the single-phase flow. However,

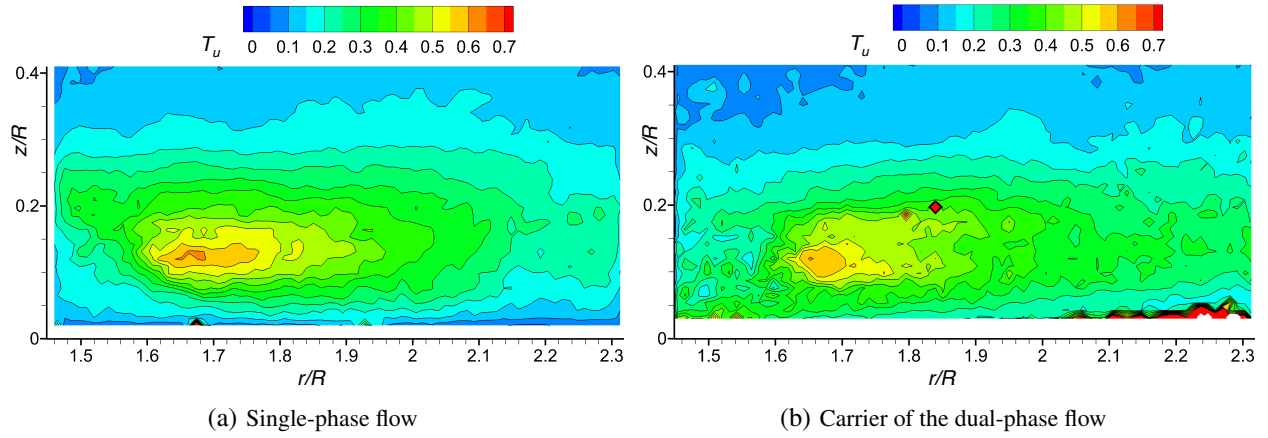


Fig. 9: Streamwise turbulence intensity, $T_u = \sqrt{u'^2}/v_h$, for the single- and dual-phase flows. (Operating conditions as defined in the text).

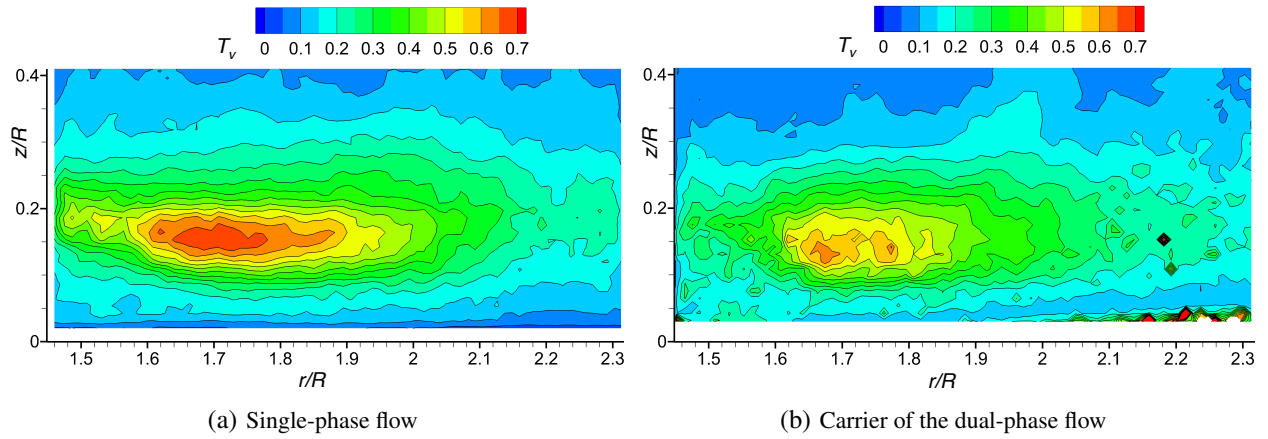


Fig. 10: Wall-normal turbulence intensity, $T_v = \sqrt{v'^2}/v_h$, for the single- and dual-phase flows. (Operating conditions as defined in the text).

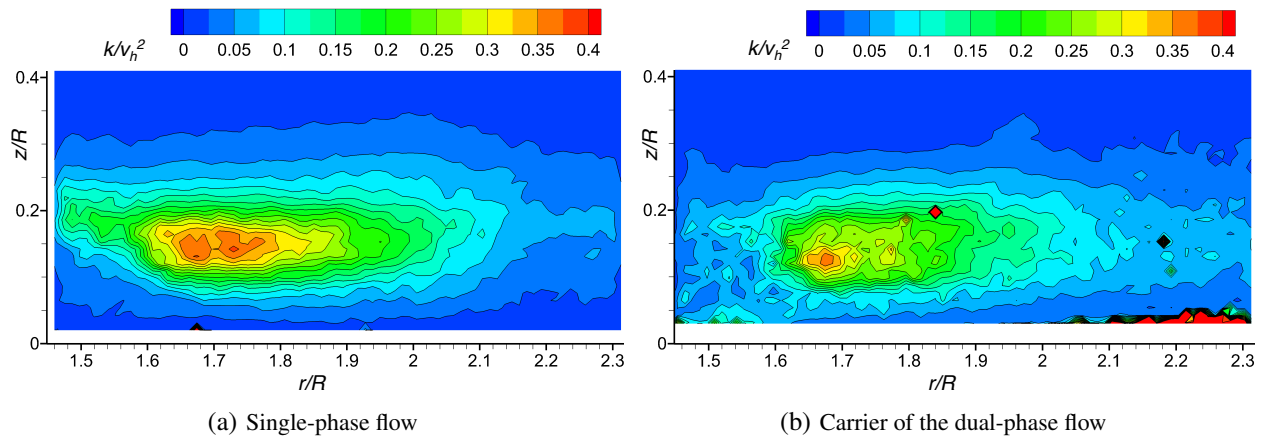


Fig. 11: Turbulent kinetic energy, k , normalized by hover induced velocity, v_h . (Operating conditions as defined in the text).

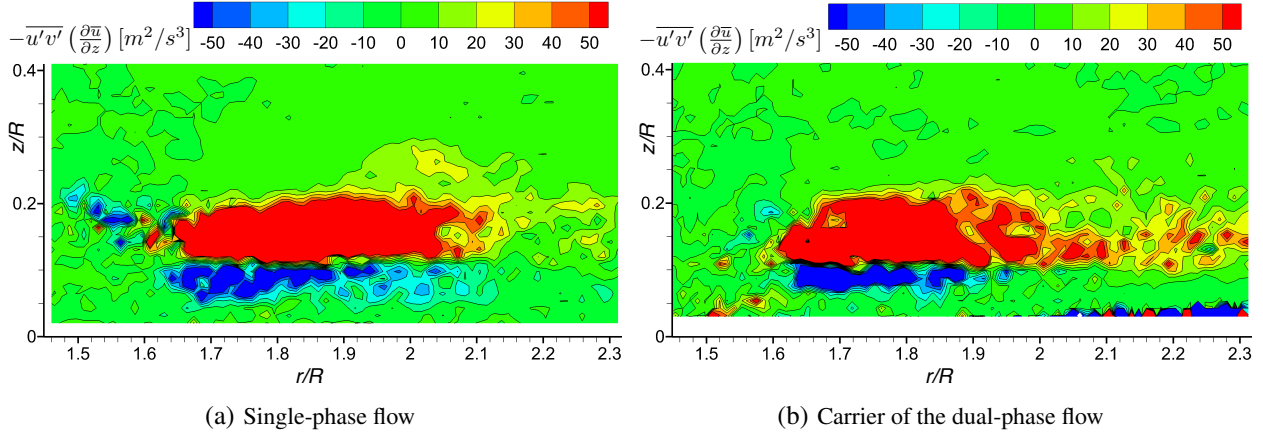


Fig. 12: Turbulence production measured in the single- and dual-phase flows. (Operating conditions as defined in the text).

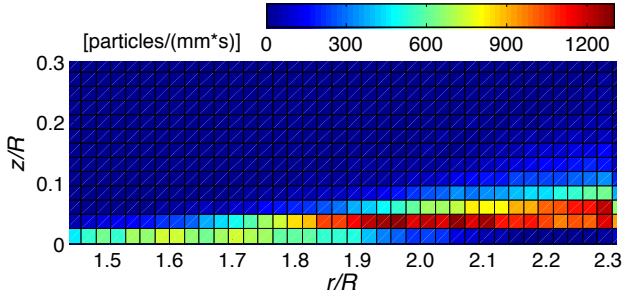


Fig. 13: Time-averaged wall-parallel particle flux.

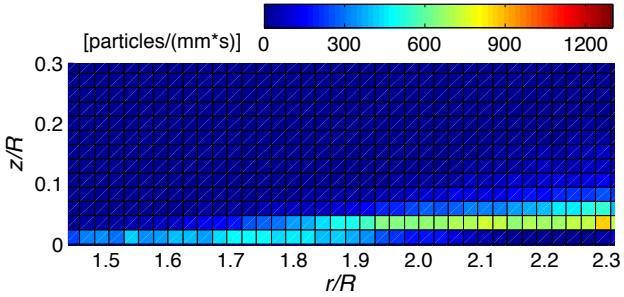


Fig. 14: Time-averaged wall-normal particle flux.

downstream of this region of intense production, the turbulence production rapidly approached zero in the single-phase flow. In contrast, the production of turbulence in the dual-phase flow environment remained at higher levels further downstream, which is the region where most sediment particles were suspended. The larger region of maximum turbulence production corresponded to the wall-normal location of the shear layer between the accelerated flow near the wall and the more quiescent flow above, and can be attributed to the combined action of the vortices and the shear layer, hence producing turbulence. Further downstream, where the tip vortices were more significantly diffused (see Fig. 8), however, additional turbulence was produced by the suspended particles themselves, as shown in Fig. 12(b).

The turbulence intensities were also examined for cuts made at the downstream location where the global maxi-

mum occurred, i.e. in this case at $r/R = 1.66$ (red lines), and also at a location further downstream where most sediment was seen to be uplifted, i.e. at $r/R = 2.26$ (blue lines); see the local particle flux in the wall-normal direction in Fig. 14. Results for the single-phase measurements (dashed lines) and for the carrier in the dual-phase measurements (solid lines) are shown for the streamwise turbulence intensity, T_u , in Fig. 15, and for the wall-normal turbulence intensity, T_v , in Fig. 16.

The dual-phase flow showed more excursions in both the vertical and streamwise turbulence intensities for the carrier-phase in the region downstream, where most sediment particles were seen to be uplifted, suspended, and transported in the flow; see Figs. 13 and 14. These excursions were seen to be more pronounced for the wall-normal turbulence (Fig. 16) than for the streamwise turbulence (Fig. 15). Furthermore, it can be observed that the wall-normal turbulence intensity, T_v , reached greater magnitudes than the streamwise component, T_u , further away from the wall, while this trend reversed as the wall was approached; also see Figs. 9 and 10. Although this finding has not been documented for a wall-bounded flow as generated by a rotor, for canonical wall-bounded flows (such as the flow over a flat plate) it is known that the turbulence in the wall-normal direction can be suppressed close to the wall [39].

Comparing the single-phase to the dual-phase results for T_u and T_v , it can be seen that the measured turbulence intensities close to the wall for both locations were greater in the dual-phase flow environment. However, this was not universally true further away from the wall (or bed) where particle concentrations were more sparse. For the upstream measurement location ($r/R = 1.66$), T_u and T_v were both greater in the single-phase flow, but only above the wall-normal distance where they reached their maximum (i.e., above $z/R \approx 0.13$). In the region downstream, where most particles were suspended, the values of T_u mostly dominated over T_v in the dual-phase flow; also compare Figs. 9(b) and 10(b). This preference in the distribution of

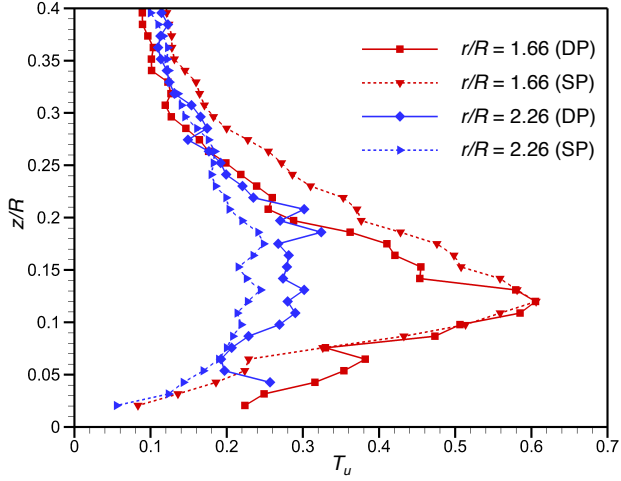


Fig. 15: Streamwise turbulence intensity for the single-phase (SP) and dual-phase (DP) flows. (Operating conditions as defined in the text).

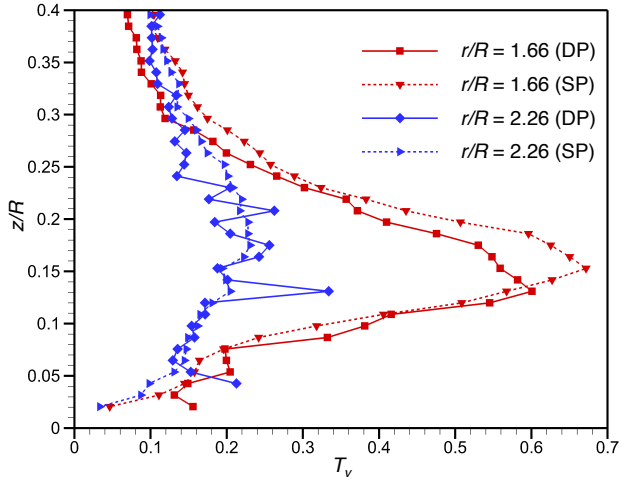
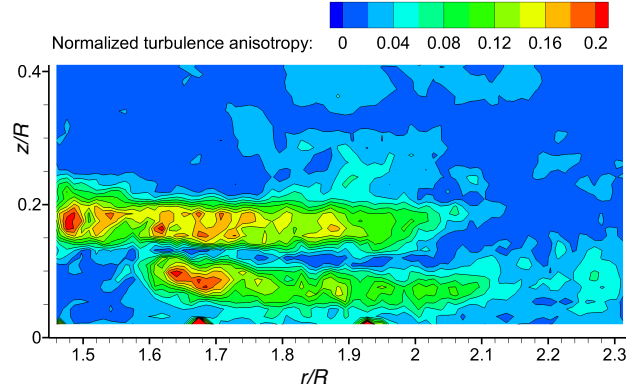


Fig. 16: Wall-normal turbulence intensity for the single-phase (SP) and dual-phase (DP) flows. (Operating conditions as defined in the text).

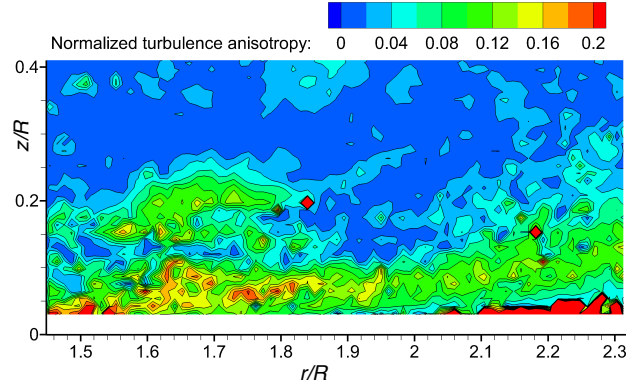
turbulence drives its anisotropy, and so the increased turbulence anisotropy in the dual-phase flow (even further away from the sediment bed) can be attributed to the increase in streamwise turbulence caused by the suspended particles; see Fig. 17(b).

4.4 Anisotropy of Turbulence

As previously discussed, the concentrated vorticity in the tip vortices induce velocity fluctuations, and hence turbulence and Reynolds stresses, and can also induce secondary vortical flows. Furthermore, the induced velocity excursions at the ground yield high shear rates. Such flow characteristics at the ground contribute to the increased anisotropy, $|\sqrt{u'^2} - \sqrt{v'^2}|/v_h$, as shown in Fig. 17. Recall that the extremely high values in Fig. 17(b) downstream of $r/R \approx 2.1$ just above the sediment bed are erroneous because of the loss of carrier-phase information when particle



(a) Single-phase flow



(b) Carrier of the dual-phase flow

Fig. 17: Turbulence anisotropy normalized by hover induced velocity, $|\sqrt{u'^2} - \sqrt{v'^2}|/v_h$. (Operating conditions as defined in the text).

concentrations are too high, causing significant laser light reflections.

Compared to the dual-phase results shown in Fig. 17(b), the turbulence near the ground showed a more isotropic distribution in the single-phase flow; see Fig. 17(a). The only source of turbulence anisotropy in the single-phase flow were the tip vortices, which convected downstream at almost a constant height above the ground (on average at a height of $z/R \approx 0.13$); this is the reason for the two elongated streaks in the streamwise direction apparent in Fig. 17. These two regions are divided by a region of relatively low values, which represents the approximate path of the vortex cores as they convected downstream.

The relatively high degree of turbulence anisotropy, even in the single-phase flow (see Fig. 17(a)) is not surprising because in highly swirling flows and stress-driven secondary flows the anisotropy of turbulence has a dominant effect on the mean flow [39]. In the dual-phase flow, turbulence anisotropy was more pronounced in proximity to the sediment bed where the highest particle fluxes were measured, and also in regions further away from the wall, but only downstream where most sediment particles were seen to be suspended in the flow; compare Fig. 17(b) to the measured particle fluxes shown in Figs. 13 and 14.

These findings confirm that particles in the flow increase

the anisotropy in the turbulence, which is consistent with results for a pipe flow [14]. Therefore, in regions where large quantities of particles are transported and airborne, the assumption of isotropic turbulence is an incorrect one for the external flow conditions of this study. Hence, turbulence models that are based on this assumption are likely to yield inadequate predictions of such a two-phase rotor flow.

5. CONCLUSIONS

Comparative single-phase and dual-phase rotor experiments were analyzed to examine how the mean flow properties, turbulence fields, and coherent vortex structures, were affected by dispersed-phase particles uplifted from a mobile sediment bed below a rotor. Contiguous time-histories of the flow generated by the rotor and the subsequent flow development over the bed were obtained with good spatio-temporal detail. The following specific conclusions have been drawn from the study:

1. The mean flow velocities and the turbulence characteristics of the rotor-generated flow near the ground were modified by the addition of the dispersed particle phase. The sediment particles were found to produce turbulence in the carrier-phase in regions that contained relatively large quantities of suspended particles.
2. The presence of sediment particles changed the vortical flow structures at the ground. In particular, the coherent tip vortex structures were distorted by the particles, resulting in the quicker radial diffusion of vorticity and, in some cases, vortex break-up. As a consequence, a more complicated vorticity field with smaller length-scales was found in the dual-phase flow environment.
3. For both the single-phase and dual-phase flows, the wall-normal turbulence intensities were found to be greater than the streamwise turbulence intensities further away from the wall, while the wall-normal component was suppressed closer to the wall (or to the sediment bed) and was consequently smaller.
4. The anisotropy of turbulence was increased by the presence of sediment particles in the dual-phase flow. This effect was found to be particularly strong near the sediment bed, in regions with increased streamwise particle flux where particles saltated along the bed and were transported downstream, and also in other regions where more sediment particles were suspended.
5. Better insight has been obtained into the approximations and boundary conditions needed for the development and validation of models for two-phase rotor-generated flows to better simulate the problem of rotorcraft brownout. Clearly, if high enough particle concentrations build up, then one-way coupling assumptions between the phases cannot be justified.

6. ACKNOWLEDGEMENTS

The Air Force Office of Scientific Research supported this work under a Multidisciplinary University Research Initiative, Grant W911NF0410176. The contract monitor was Dr. Douglas Smith.

REFERENCES

- [1] Mapes, P., Kent, R., and Wood, R., "DoD Helicopter Mishaps FY85-05: Findings and Recommendations," U.S. Air Force, 2008.
- [2] National Transportation Safety Board, NTSB Accident Briefs: LAX01LA283, LAX01LA304, LAX04LA285, SEA05CA173.
- [3] Leishman, J. G., "Challenges in Understanding the Fluid Dynamics of Brownout: Review and Update," Proceedings of the AHS International Meeting on Advanced Rotorcraft Technology and Safety Operations, Omiya, Japan, November 1–3, 2010.
- [4] Rauleder, J., and Leishman, J. G., "Measurements of the Turbulent Flow Environment on the Ground Below a Hovering Rotor," 37th European Rotorcraft Forum, Italy, September 13–15, 2011.
- [5] Milluzzo, J., Sydney, A., Rauleder, J., and Leishman, J. G., "In-Ground-Effect Aerodynamics of Rotors with Different Blade Tips, American Helicopter Society 66th Annual Forum Proceedings, Phoenix, AZ, May 10–13, 2010.
- [6] Syal, M., Rauleder, J., Tritschler, J. K., and Leishman, J. G., "On the Possibilities of Brownout Mitigation Using a Slotted-Tip Rotor Blade," 29th AIAA Applied Aerodynamics Conference, Honolulu, HI, June 27–30, 2011.
- [7] Tritschler, J. K., Syal, M., Celi, R., and Leishman, J. G., "The Effect of Number of Blades on Optimum Rotor Design for Brownout Mitigation," Future Vertical Lift Aircraft Design Conference, San Francisco, CA, January 18–20, 2012.
- [8] Lee, T. E., Leishman, J. G., and Ramasamy, M., "Fluid Dynamics of Interacting Blade Tip Vortices With a Ground Plane," *Journal of the American Helicopter Society*, Vol. 55, 022005, 2010, DOI:10.4050/JAHS.55.022005.
- [9] Nathan, N. D., and Green R. B., "Measurements of a Rotor Flow in Ground Effect and Visualisation of the Brownout Phenomenon," American Helicopter Society 64th Annual Forum Proceedings, Montréal, Canada, April 29–May 1, 2008.
- [10] Johnson, B., Leishman, J. G., and Sydney, A., "Investigation of Sediment Entrainment in Brownout Using High-Speed Particle Image Velocimetry," *Journal of the American Helicopter Society*, Vol. 55, 042003, 2010, DOI:10.4050/JAHS.55.042003.

- [11] Sydney, A., Baharani, A., and Leishman, J. G., "Understanding Brownout Using Near-Wall High-Speed Dual-Phase Flow Measurements," American Helicopter Society 67th Annual Forum Proceedings, Virginia Beach, VA, May 3–5, 2011.
- [12] Rauleder, J., and Leishman, J. G., "Flow Environment and Organized Turbulence Structures at the Ground Below a Rotor," American Helicopter Society 68th Annual Forum Proceedings, Fort Worth, TX, May 1–3, 2012.
- [13] Syal, M., Govindarajan, B., and Leishman, J. G., "Mesoscale Sediment Tracking Methodology to Analyze Brownout Cloud Developments," American Helicopter Society 66th Annual Forum Proceedings, Phoenix, AZ, May 10–13, 2010.
- [14] Poelma, C., Westerweel, J., and Ooms, G., "Particle-Fluid Interactions in Grid-Generated Turbulence," *Journal of Fluid Mechanics*, Vol. 589, 2007, pp. 315–351.
- [15] Poelma, C., and Ooms, G., "Particle-Turbulence Interaction in a Homogeneous, Isotropic Turbulent Suspension," *Applied Mechanics Reviews*, Vol. 59, 2006, pp. 78–90.
- [16] Kaftori, D., Hesteroni, G., and Banerjee, S., "The Effect of Particles on Wall Turbulence," *International Journal of Multiphase Flow*, Vol. 24, (3), 1998, pp. 359–386.
- [17] Mulinti, R., and Kiger, K., "Two-Phase PIV Measurements of Particle Suspension in a Forced Impinging Jet," 63rd Annual Meeting of the APS Division of Fluid Dynamics, Vol. 55, (16), November 21–23, 2010, Long Beach, CA.
- [18] Unadkat, H., Rielly, C. D., Hargrave, G. K., and Nagy, Z. K., "Application of Fluorescent PIV and Digital Image Analysis to Measure Turbulence Properties of Solid-Liquid Stirred Suspensions" *Chemical Engineering Research and Design*, Vol. 87, 2009, pp. 573–586.
- [19] Montante, G., and Magelli, F., "Mixed Solids Distribution in Stirred Vessels: Experiments and Computational Fluid Dynamics Simulations," *Industrial & Engineering Chemical Research*, Vol. 46, 2007, pp. 2885–2891.
- [20] Kulick, J. D., Fessler, J. R., and Eaton, J. K., "Particle Response and Turbulence Modification in Fully Developed Channel Flow," *Journal of Fluid Mechanics*, Vol. 277, 1994, pp. 109–134.
- [21] Kiger, K. T., and Pan, C., "Suspension and Turbulence Modification Effects of Solid Particulates on a Horizontal Turbulent Channel Flow," *Journal of Turbulence*, Vol. 19, (3), 2002.
- [22] Zhang, W., Wang, Y., and Lee, S. J., "Simultaneous PIV and PTV Measurements of Wind and Sand Particle Velocities," *Experiments in Fluids*, Vol. 45, 2008, pp. 241–256.
- [23] Bagnold, R. A., *The Physics of Blown Sand and Desert Dunes*, Dover Publications, Inc., Mineola, NY, 1941.
- [24] Sterk, G., Jacobs, A., and Van Boxel, J., "The Effect of Turbulent Flow Structures On Saltation Sand Transport in the Atmospheric Boundary Layer," *Earth Surface Processes and Landforms*, Vol. 23, 1998, pp. 877–887.
- [25] Sterk, G., Van Boxel, J., and Zuurbier, R., "Interactions Between Turbulent Wind Flow and Saltation Sand Transport," ICAR5/GCTE-SEN Joint Conference Proceedings, Lubbock, TX, July 22–25, 2002.
- [26] Clifford, N. J., McClatchey, J., and French, J. R., "Measurements of Turbulence in the Benthic Boundary Layer Over a Gravel Bed and Comparison Between Acoustic Measurements and Predictions of the Bedload Transport of Marine Gravels," *Sedimentology*, Vol. 38, 1991, pp. 161–171.
- [27] Sutherland, A., "Proposed Mechanism for Sediment Entrainment by Turbulent Flows," *Journal of Geophysical Research*, Vol. 72, 1967, pp. 6183–6194.
- [28] Xuan, J., "Turbulence Factors for Threshold Velocity and Emission Rate of Atmospheric Mineral Dust," *Atmospheric Environment*, Vol. 38, 2004, pp. 1777–1783.
- [29] Shao Y., and Lu, H., "A Simple Expression for Wind Erosion Threshold Friction Velocity," *Journal of Geophysical Research*, Vol. 105, (D17), 2000, pp. 22,437–22,443.
- [30] Williams, J. J., Butterfield, G. R., and Clark, D. G., "Rates of Aerodynamic Entrainment in a Developing Boundary Layer," *Sedimentology*, Vol. 37, 1990, pp. 1039–1048.
- [31] Xuan, J., and Robins, A., "The Effects of Turbulence and Complex Terrain on Dust Emissions and Depositions from Coal Stockpiles," *Atmospheric Environment*, Vol. 28, 1994, pp. 1951–1960.
- [32] Leishman, J. G., *Principles of Helicopter Aerodynamics*, Cambridge University Press, New York, NY, 2006.
- [33] Ramasamy, M., Johnson, B., and Leishman, J. G., "Turbulent Tip Vortex Measurements Using Dual-Plane Stereoscopic Particle Image Velocimetry," *AIAA Journal*, 2009, Vol. 47, (8), pp. 1826–1840.
- [34] Geiser, J., and Kiger, K., "A Simplified Analog for a Rotorcraft-in-Ground-Effect Flow Using a Forced Impinging Jet," 63rd Annual Meeting of the APS Division of Fluid Dynamics, Vol. 55, (16), November 21–23, 2010, Long Beach, CA.
- [35] Elghobashi, S., "On Predicting Particle-Laden Turbulent Flows," *Journal of Applied Sciences Research*, Vol. 52, 1994, pp. 309–329.

[36] Irwin, H. P. A. H., "Measurements in a Self-Preserving Plane Wall Jet in a Positive Pressure Gradient," *Journal of Fluid Mechanics*, Vol. 61, (1), 1973, pp. 33–63.

[37] Robinson, S. K., "Coherent Motions in the Turbulent Boundary Layer," *Annual Review of Fluid Mechanics*, Vol. 23, 1991, pp. 601–639.

[38] Eaton, J. K., "Turbulence Modification by Particles in Shear Flows," ASME FED-228, Gas Particle Flows.

[39] Bernard, P. S., and Wallace, J. M., *Turbulent Flow: Measurement, Analysis and Prediction*, John Wiley & Sons, Inc., New York, 2002.